



ORIGINAL ARTICLE

Synthesis of 2D boron nitride doped polyaniline hybrid nanocomposites for photocatalytic degradation of carcinogenic dyes from aqueous solution

Syed Shahabuddin ^{a,*}, Rashmin Khanam ^b, Mohammad Khalid ^c,
Norazilawati Muhamad Sarih ^c, Juan Joon Ching ^d, Sharifah Mohamad ^e,
R. Saidur ^{a,f,*}

^a Research Centre for Nano-Materials and Energy Technology (RCNMET), School of Science and Technology, Sunway University, 47500 Selangor Darul Ehsan, Malaysia

^b Centre for Interdisciplinary Research in Basic Sciences, Jamia Millia Islamia, New Delhi 110025, India

^c Department of Chemistry, Faculty of Science, University of Malaya, 50603 Kuala Lumpur, Malaysia

^d Nanotechnology & Catalysis Research Centre, University of Malaya, 50603 Kuala Lumpur, Malaysia

^e Graphene & Advanced 2D Materials Research Group (GAMRG), Research Centre for Nano-materials and Energy Technology (RCNMET), School of Science and Technology, Sunway University, No. 5, Jalan Universiti, Bandar Sunway, 47500 Subang Jaya, Selangor, Malaysia

^f Department of Engineering, Lancaster University, Lancaster, LA14YW, UK

Received 7 May 2018; accepted 8 May 2018

Available online 19 May 2018

KEYWORDS

Boron nitride;
Polyaniline;
Nanocomposite;
Photocatalysis;
Dyes

Abstract This investigation focused on the photocatalytic treatment of pollutants in waste water using methylene blue (MB) and methyl orange (MO) as the model dyes. In this study, conducting polyaniline (PANI) based nanocomposites doped with 2D hexagonal boron nitride (h-BN) were synthesised using simplistic oxidative in-situ polymerization technique by employing ammonium persulfate as an initiator in acidic medium. The synthesised 2D h-BN doped PANI nanocomposites were comprehensively characterized using field emission scanning electron microscopy (FESEM), transmission electron microscopy (TEM), elemental mapping, X-ray diffraction (XRD), Brunauer-Emmett-Teller analysis (BET), thermogravimetric analysis (TGA), and Fourier trans-

* Corresponding authors at: Research Centre for Nano-Materials and Energy Technology (RCNMET), School of Science and Technology, Sunway University, 47500 Selangor Darul Ehsan, Malaysia.

E-mail addresses: syeds@sunway.edu.my, syedshahab.hyd@gmail.com (S. Shahabuddin), saidur@sunway.edu.my (R. Saidur).

Peer review under responsibility of King Saud University.



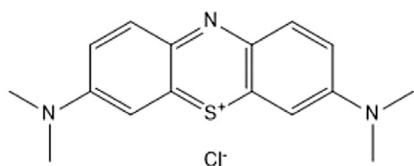
Production and hosting by Elsevier

form infrared spectroscopy (FTIR). Degradation of MB and MO dyes under UV irradiations was performed to evaluate the photocatalytic performance of the synthesised nanocomposites. The results indicated that the h-BN nanosheets doped nanocomposites demonstrated better photocatalytic activities as compared to bare PANI or h-BN. Moreover, the nanocomposite P-BN-2, with 2 wt% of 2D h-BN nanosheets was found to be an optimal composition with 93% and 95% degradation efficiency for MB and MO within 90 min respectively.

© 2018 The Authors. Production and hosting by Elsevier B.V. on behalf of King Saud University. This is an open access article under the CC BY-NC-ND license (<http://creativecommons.org/licenses/by-nc-nd/4.0/>).

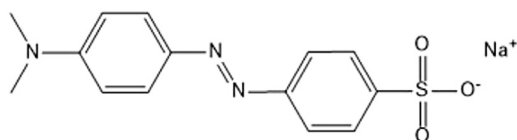
1. Introduction

The current era is the age of rapid industrialization which has witnessed a rapid development and is a major contributing factor to environmental degradation. Environmental pollution has been a serious issue which has attracted considerable attention due to its negative impact on the ecosystem and has been centre of immense scientific consideration (Xing et al., 2017; Ge et al., 2016; Syed, 2016; Snyder et al., 2013). Water bodies are one of the major sufferer of environmental pollution since the organic pollutants such as dyes are often discharged from various industries including textile, food industries directly into the water bodies and causes severe water pollution (Shahabuddin et al., 2016a). The coloured dyes effluents are often non-biodegradable (Raffainer and Rudolf von Rohr, 2001) which effects the aquatic flora and fauna as they reduce the penetration of solar radiations thereby effecting photosynthetic activities (Gupta, 2009) besides being toxic and carcinogenic for human beings (Shahabuddin et al., 2016b; McCann and Ames, 1976). According to the World bank assessment, approximately 10–15% of the organic coloured dyes are discarded into the water bodies from dyeing industries contributing around 17–20% of the total industrial aqueous pollution (Chan et al., 2011; Huang et al., 2014; Shahabuddin et al., 2016c). 3,7-Bis(dimethylamino)-phenothiazin-5-ium chloride and Sodium 4-((4-dimethylamino)-phenyldiazenyl)-benzenesulfonate, commonly known as methylene blue (MB) and methyl orange (MO), are commonly used synthetic dyes with the complex



3,7-Bis(dimethylamino)-phenothiazin-5-ium chloride

Methylene blue (MB)



Sodium 4-((4-dimethylamino)-phenyldiazenyl)-benzenesulfonate

Methyl orange (MO)

Scheme 1 Chemical structures of Methylene blue and Methyl orange.

chemical structures as depicted in Scheme 1. These dyes are often used in various industrial applications including food, textiles, paper, laser printing, additives and are known to be highly stable, persistent and terribly harmful for living beings in higher concentrations (Parida et al., 2010; Shahabuddin et al., 2015). The harmful effects of dyes effluents to human being includes quadriplegia, jaundice, cyanosis, diarrhoea, tissue necrosis, vomiting and may be carcinogenic in extreme cases (Gouamid et al., 2013; Vinothkannan et al., 2015; Adams et al., 2007). Thus, there is an immense need to develop techniques which can address the challenge posed by these aforementioned pollutants. Among various techniques developed to degrade harmful pollutants from waste water, photocatalysis has proved to be most effective method to transform the toxic complex organic pollutants into the less toxic or even completely harmless molecules by utilising simple light energy from sunlight or UV illumination (Shahabuddin et al., 2016a, 2015; Dai et al., 2014).

Currently, conducting polymeric based nanomaterials have appeared as plausible substitutes to traditional nanomaterials owing to their tuneable surface chemistry, enhanced mechanical stability, larger surface area, uniform pore size distribution, and possible regeneration under minor conditions (Zare et al., 2018; Nodeh et al., 2018). Due to their unique π -conjugated electron systems in polymeric backbone, conducting polymers possess unique optoelectronic and electrical properties. Recently, conducting polymer based nanocomposites comprising polyaniline (PANI), polythiophene (PTh), polyethelamine (PEI), polypyrrole (PPy), etc. have gain considerable scientific attention in wide varieties of applications such as photocatalysis, sensors, adsorbents, thermoelectric, electromagnetic, batteries, electro-luminescence, and electromechanical applications (Shahabuddin et al., 2016b, 2016c; Zare et al., 2018; Jamal et al., 2016; Srivastava et al., 2015; Baharin et al., 2016). Amongst all the conducting polymers, polyaniline (PANI) is extensively explored due to its cost effectiveness, facile synthetic methodologies, unique porous surface, ease of regeneration, mechanical and environmental robustness, insolubility in water and non-toxicity (Shahabuddin et al., 2016a; Zare et al., 2018). PANI is usually used as a conjugated conductive polymer which is polymerised with wide band gap inorganic semiconducting metal oxides, sulphides, etc. and demonstrates explicit photocatalytic, optical, and photoelectric properties (Gustafsson et al., 1992; Jang et al., 2000). In addition to the above-mentioned properties, PANI also acts as an efficient electron donor and an eminent hole transporter when it is subjected to UV-visible irradiation. The composite material of PANI with a high band gap metal oxide possess unique electron transfer mechanism where PANI can generate electrons upon photon irradiation and can transfer these photogenerated electrons to the conduction band of the semiconducting metal oxide such as SrTiO₃, TiO₂, ZnO. This transfer of

electron is possible since the LUMO (lowest unoccupied molecular orbital) of PANI is higher in energy level than the conduction band (CB) of metal oxides (Shahabuddin et al., 2016; Wang et al., 2010). This results in considerable volume of interfacial charge transfer and significant reduction in the recombination of electron-hole pair which may perhaps afford a substantial photoresponse upon photoexcitation.

Inorganic metal oxides, sulphides, nitrides, etc. have been potentially used as dopant materials with conducting polymers to design unique nanocomposites with interesting properties. Nanocomposites comprising of inorganic materials and conductive polymers have been extensively explored in the field of photocatalysis since these composite materials had exhibited enhanced photocatalytic activities. The semiconducting nature of metal oxides is an essential feature which makes them as photosensitisers in photochemical reaction due to their empty conduction bands (CB) and filled valence bands (VB). Among various conducting polymers, PANI has been significantly explored with various types of inorganic metal oxides such as SrTiO₃, TiO₂, ZnS, ZnO, Co₃O₄ since it possesses enhanced electron mobility whereby the electrons are easily excited under photo illumination (Golsheikh et al., 2015; Ray and Biswas, 2000; Autin et al., 2013; Singh, 2010). The photoelectrons generated in the excited antibonding orbitals (π^*) of the PANI matrix transfer into the empty conduction band of these inorganic metal oxides and sulphides (Zhang et al., 2006). These electrons and holes reacts with the surrounding water and oxygen molecules to form superoxide and hydroxide radicals which are responsible for photodegradation of the organic molecules. Two-dimensional semiconducting materials owing to their fundamental and unique surface properties have been widely explored in various applications (Guo et al., 2013). Among various 2D materials, hexagonal boron nitride (h-BN) has gained vast scientific attention due to its structural similarity with graphene and interesting chemical and physical properties such as enhanced thermal stability, excellent thermal conductivity, higher band gap, chemically resistant, and higher surface area (Jang et al., 2016; Kim et al., 2012; Salehirad and Nikje, 2017). h-BN is a covalently bonded, hexagonal crystalline layered compound of boron and nitrogen where the B and N atoms arranged in a sp² hybridized honeycomb lattice resembling graphene (Nag et al., 2010; Song et al., 2012). 2D h-BN nanosheets have larger surface area and exhibited greater electron and phonon transport as compared with their 0D and 1D counterparts (Salehirad and Nikje, 2017; Bhimanapati et al., 2016). Thus h-BN appeared to be an interesting material for photosensitization of conductive PANI an area which has not been much explored.

Herein, we report the facile synthesis of PANI nanotubes and 2D h-BN doped PANI nanotubes through simplistic in-situ oxidative polymerization for the photocatalytic degradation of carcinogenic MB and MO dyes from aqueous solution. 2D h-BN was incorporated into the conducting PANI nanotubes during polymerization of aniline monomer. PANI was selected as a matrix material for designing the photocatalyst based upon its cost effectiveness, significantly enhanced electron mobility, easy excitation of electrons through photo irradiations and facile method of synthesis. Moreover, doping of PANI nanotubes with h-BN nanosheets synergistically augments the generation of photoelectrons and holes which has overall increased the photocatalytic efficiency of the nanocomposites. The photocatalytic efficiency of the synthesised nanocomposites

was evaluated by investigating the degradation of MB and MO under UV irradiations spectrophotometrically. The optimised amount of 2D h-BN nanosheets within the PANI nanotubes matrix was found to 2 wt% with respect to aniline with 93% and 95% degradation of MB and MO respectively in 90 min. Simplistic synthesis methodology, cost-effectiveness and enhanced photocatalytic degradation performance make these 2D h-BN nanosheets doped polyaniline nanocomposites as the credible photocatalysts for organic dyes degradation.

2. Experimental section

2.1. Materials

Under reduced pressure distillation of Aniline (Fluka, $\geq 99\%$) was performed followed by its storage in the dark prior to its use. Other necessary chemicals including ammonium peroxydisulfate, APS (Merck, $\geq 99\%$) HCl (Merck, 37%); methanol (Merck, 99.9%) and acetone (Merck, 95%) were used without any further purification. Hexagonal boron nitride (h-BN) powder having an average particle size of 70 nm was procured from Lower Friction Company (Canada). All the analytical grade reagents were used in all the experiments. Deionised water was used throughout the entire study.

2.2. Preparation of polyaniline nanotubes (PANI)

Oxidative polymerisation of distilled aniline was employed in aqueous HCl (1M) by taking ammonium persulfate (APS) as an oxidant to synthesise polyaniline nanotubes. In short, 0.0215 mol of aniline was taken in 30 mL of 1 M of HCl (aq.) solution. The oxidant solution was added gradually to the aniline solution maintaining rate of one drop per second while stirring continuously at 0–5 °C. Stirring was continued for another 3hrs and kept overnight in refrigerator for allowing completion of reaction. Followed by this, the reaction mixture was subjected to filtration and washing using HCl (0.5 M) up until the filtrate become colourless and successively with deionized water to make the filtrate neutral. Subsequently, the obtained product was washed using solvent 1:1 mixture of acetone and methanol to remove all unreacted monomers and oligomers. The resultant polymer was dried overnight by keeping in vacuum oven at pressure of 100 mb and 60 °C. The appearance of green colour of the resultant polymer specified the formation of conductive polyaniline emeraldine salt.

2.3. Preparation of PANI-h-BN nanocomposite

Synthesis of h-BN nanosheets doped nanocomposites were carried out using various wt% of h-BN (1, 2 and 5 wt% with respect to 0.0215 mol of aniline). Calculated amount of h-BN nanosheets were dispersed in 5 mL of deionised water by sonication and added dropwise to aniline solution in HCl with vigorous stirring. The resultant reaction mixture was sonicated for a few minutes until it became uniform. The protocol for further work up was similar to described in the above section. The nanocomposites so obtained were labelled as P-BN-1, P-BN-2 and P-BN-5 specifying 1, 2, and 5 wt% of h-BN nanosheets with respect to aniline, respectively. The experimental set up for the synthesis of nanocomposites from monomer is depicted in Fig. S1.

2.4. Characterisation techniques

JEOL JSM-7600F field emission scanning electron microscope functioning at 10 kV was used to evaluate the surface morphological and elemental analysis of the synthesised product. JEOL JEM-2100F high-resolution transmission electron microscope was used to study the size, shape and crystallinity of the prepared nanocomposites. Perkin Elmer TGA6 was employed to investigate the thermal stability under nitrogen atmosphere having heating rate of 10 °C/min. 10 mg of dried sample was kept inside the alumina crucible, and the weight changes were assessed within the temperature range of 35 °C to 900 °C. Empyrean X-ray diffractometer was used to record the X-ray diffraction (XRD) patterns by keeping the $2\theta = 10\text{--}90^\circ$ using Cu K α radiations ($\lambda = 1.5418 \text{ \AA}$) at a scan rate of 0.02 s $^{-1}$. Micromeritics Tristar II ASAP 2020 system was used to carry out analysis of surface area using by nitrogen adsorption/desorption isotherms at 77 K. Brunauer-Emmett-Teller (BET) methods was employed to measure the specific surface areas. Perkin Elmer RX1 FT-IR ATR spectrometer within range of 400–4000 cm $^{-1}$ was used to obtain the FT-IR spectra of the synthesized samples using KBr pellets.

2.5. Measurement of photocatalytic activities

To evaluate the photocatalytic activities of the synthesized samples, degradation of methylene blue (MB) and methylene orange (MO) dye were monitored in the aqueous phase. About

20 mg of the synthesized nanocomposite powder was dispersed in 100 mL of an aqueous dye solution having starting concentration of 10 mg L $^{-1}$ in quartz vessel. By stirring the reaction mixture for about 60 min in the dark environment, the adsorption-desorption equilibrium was attained. The photocatalytic degradation was then conducted by irradiating the above mixture using a UV source placed at a distance of 3 cm from solution. To achieve uniformity in dispersion of photocatalyst particles, the dye solution along with photocatalyst was bubbled with air followed by continuous stirring. The arrangement of photocatalytic setup is depicted in Fig. S2. Thereafter, 3 mL of the dye suspension was withdrawn at a regular time interval and centrifuged. The UV-visible absorption spectra of the supernatant solution were analysed using a UV-visible spectrometer in 1 cm quartz cuvettes to evaluate the characteristic absorption peak of MB and MO.

3. Results and discussion

3.1. Morphological analysis of nanocomposites

Morphological analysis of the h-BN nanosheets, PANI nanotubes, and h-BN nanosheets doped PANI nanocomposites were comprehensively studied by FESEM and TEM techniques. Fig. 1(a) and (b) depicts the surface morphology of h-BN nanosheets. As evident from the Fig. 1(a), h-BN revealed the discs like morphology in nano-range. These disc shaped h-BN nanosheets are highly stacked as illustrated by Fig. 1(b).

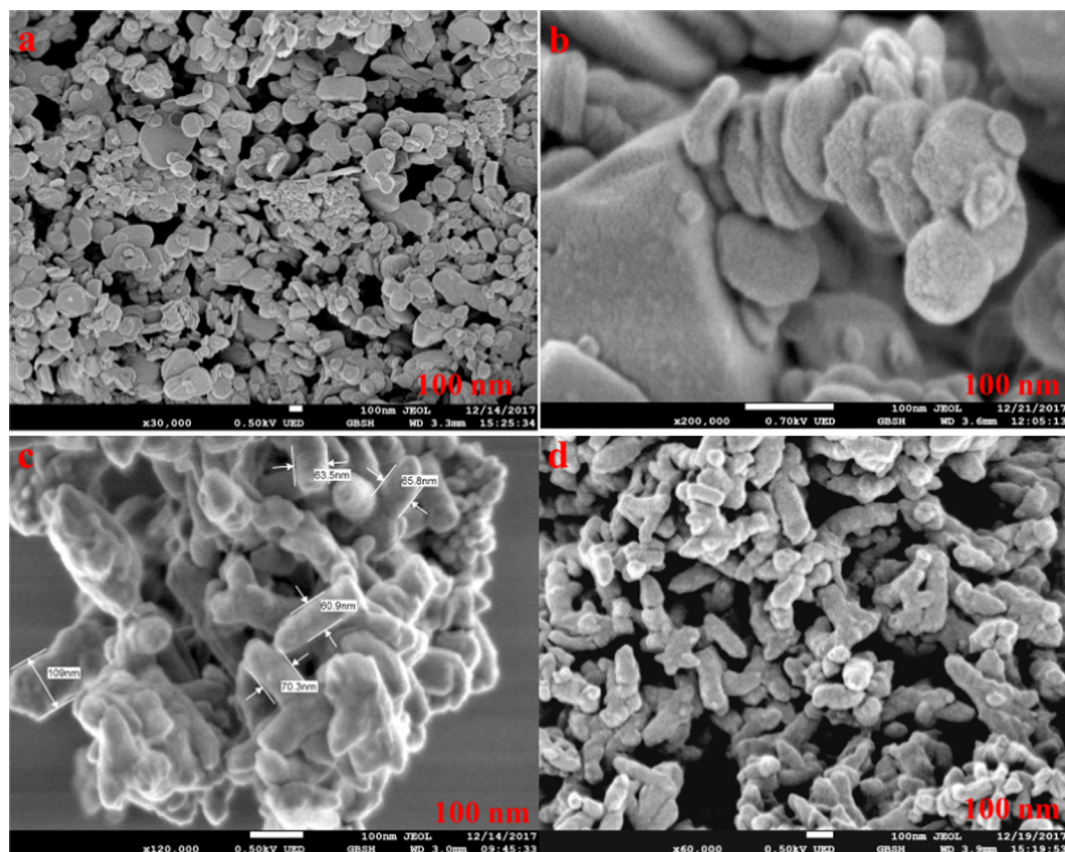


Fig. 1 FESEM micrographs of (a and b) h-BN (c) PANI, and (d) P-BN-5.

The FESEM micrograph of PANI is depicted in Fig. 1(c). As obvious from the figure, PANI exhibited well defined tubular morphology and the measurements of the tubes confirms the formation of nanotubes. Surface morphological analysis of h-BN nanosheet doped nanocomposite, P-BN-5, clearly demonstrate the transformation in the PANI nanotubes into granular polymeric network Figs. 1(d) and S1). The addition of h-BN nanosheets does not have much impact on the morphology of PANI polymer but the surface has been modified to much granular as evident by the highly magnified nanocomposite image depicted in Fig. S3. However, it is difficult to visualise the h-BN nanosheets in the nanocomposites since the concentration of the former is very meagre as compared to PANI nanotubes.

In order to further confirm the formation of nanocomposites, TEM analysis were performed for h-BN nanosheets, PANI nanotubes and h-BN nanosheets doped nanocomposites, P-BN-5. Fig. 2 demonstrates the TEM micrographs of h-BN nanosheets, PANI nanotubes whereas Fig. 3 demonstrates the TEM image of P-BN-5 nanocomposite. TEM image h-BN nanosheet is illustrated in Fig. 2(a) which clearly reveals the disc shaped morphology. The HRTEM image of h-BN is represented in Fig. 2(b) which clearly shows the layered structures with the interlayer distance measured to be 2.5 Å, which is the characteristic N-N intralayer distance in h-BN lattice (Kim et al., 2011; Kobayashi and Akasaka, 2008). Fig. 2(b) displays the in-plane high-resolution selected area electron diffraction (SAED) pattern of h-BN nanosheets depicting the

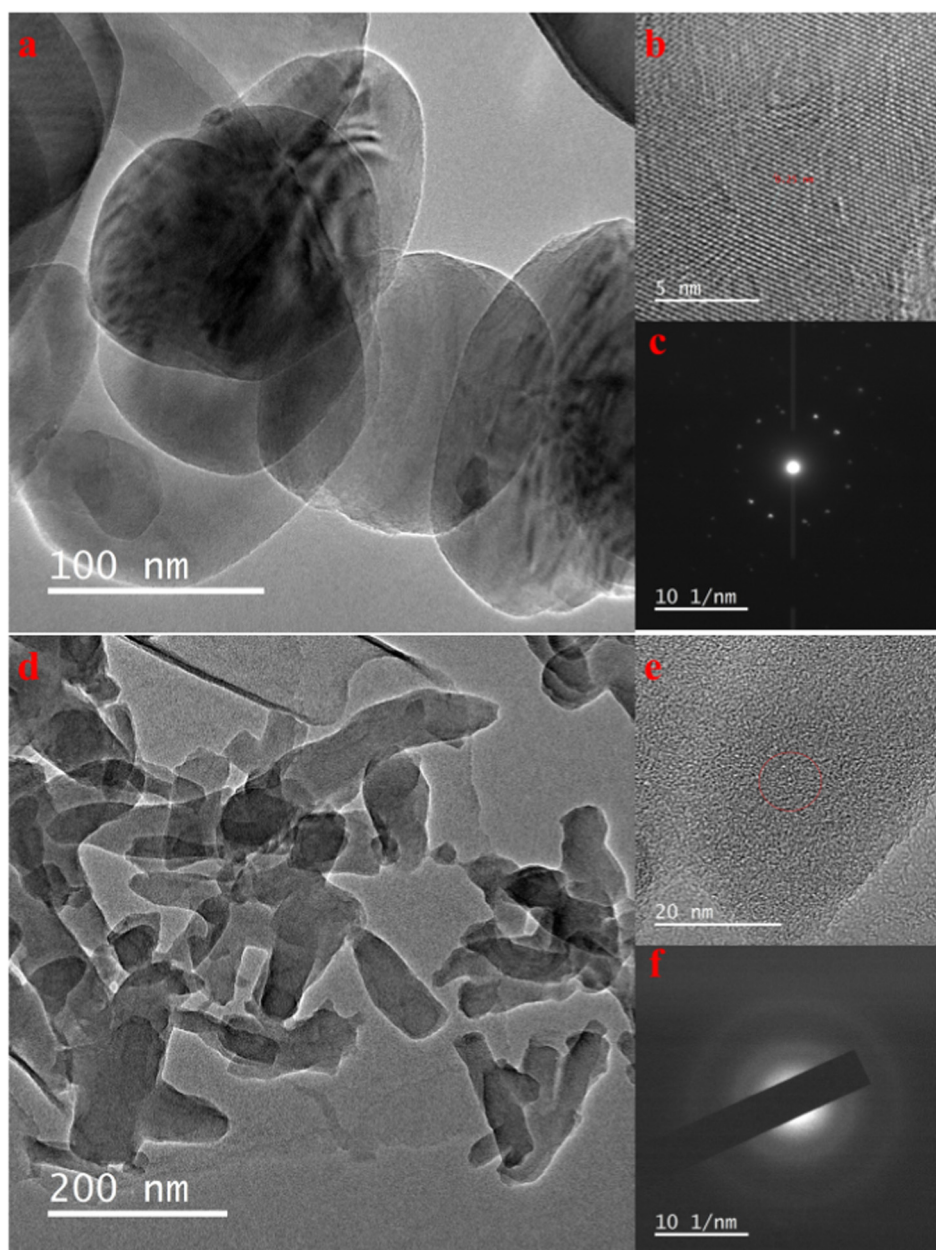


Fig. 2 (a–b) HRTEM images of h-BN nanosheets (c) SAED pattern for h-BN (d–e) HRTEM images of PANI nanotubes and (f) SAED pattern for PANI nanotubes.

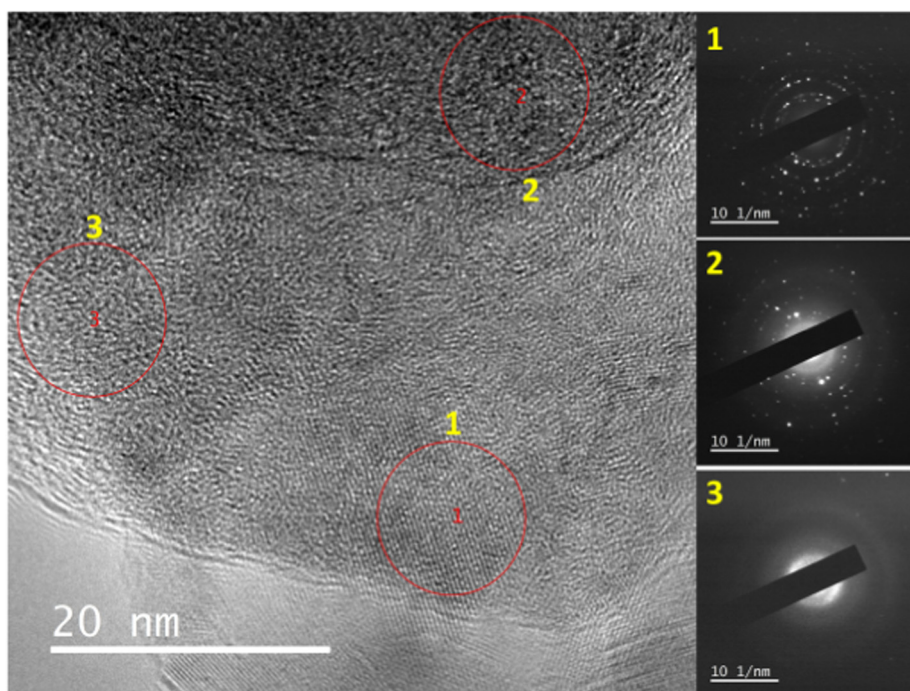


Fig. 3 HRTEM image of P-BN-5 nanocomposites with SAED pattern at three different points.

polycrystalline in-plane structures in the h-BN nanosheets (Jang et al., 2016). As apparent from Fig. 2(d), formation of PANI nanotubes is confirmed by TEM micrograph. Fig. 2(e) and (f) represents the high resolution TEM image and selected area electron diffraction (SAED) pattern for PANI nanotubes which clearly reveals the formation of pure amorphous polymeric material with no crystalline phase. In order to observe the presence of h-BN polycrystalline phase in amorphous polymer matrix, high resolution TEM analysis was performed for nanocomposite, P-BN-5 as illustrated in Fig. 3. As noticeable from Fig. 3, the selected area electron diffraction (SAED) pattern were taken from three different spots namely spot 1, 2 and 3. The SAED analysis indicates the presence h-BN with the matrix of amorphous PANI. Thus, FESEM and TEM analysis clearly reveals the formation PANI nanotubes and h-BN nanosheets doped nanocomposite.

Additionally, as the amount h-BN nanosheets is very less as compared to the bare polymer matrix and these sheets are embedded deep within the polymer matrix, it is difficult to observe the uniform presence of h-BN in PANI matrix by using FESEM or TEM alone. In order to demonstrate the uniform presence of h-BN within the PANI matrix FESEM elemental mapping technique was employed. Fig. 4 exhibits the elemental mapping result of P-BN-2 nanocomposite with 2 wt% h-BN. As can be seen from the obtained results, boron and nitrogen are uniformly present within the polymer matrix along with carbon, chlorine and oxygen thereby confirming the formation of h-BN nanosheet nanocomposite with uniform distribution of h-BN.

3.2. Thermal analysis

Thermogravimetric analysis of the h-BN, PANI nanotubes, and h-BN doped PANI nanocomposites were performed at

the thermal range of 30 °C to 900 °C with a ramp rate of 10 °C/min under inert nitrogen atmosphere. Fig. 5 epitomises the thermal investigation of h-BN, PANI nanotubes and h-BN doped nanocomposites namely P-BN-1, P-BN-2 and P-BN-5. As revealed by the thermogram of h-BN, only a minor weight loss of 1.6% was observed from the temperature range of 35–900 °C which illustrates that h-BN is highly stable at elevated temperatures. The thermogram of PANI nanotubes demonstrated three principal weight losses at the heating range of 35–900 °C. Initially PANI nanotubes exhibited a prominent weight loss from 40 to 130 °C, which might be due to the removal of moisture adsorbed within polymer matrix, disintegration of the unreacted aniline monomer and decomposition of the impurities (Syed, 2016; Shahabuddin et al., 2015). Another major weight loss appeared around 130–300 °C which can be assigned to the loss of dopant molecules from polymeric backbone and finally another weight loss was noticed from 300 to 900 °C which is attributed to the breakdown and decomposition of the carbonaceous polymeric chains (Mostafaei and Zolriasatein, 2012). The thermogram of the h-BN nanosheets doped nanocomposites revealed enhanced stability as compared to the bare PANI nanotubes which may be due to the presence of thermally stable pure h-BN nanosheets in the nanocomposite material. Hence, the thermal investigation of the nanocomposites evidently indicates the enhancement in the thermal stability of P-BN-1, P-BN-2 and P-BN-5 owing to the presence of thermally stable pure h-BN nanosheets within the polymeric matrix and this stability increases with increasing the percentage of h-BN in nanocomposites.

3.3. BET analysis

Brunauer-Emmett-Teller (BET) analysis is one of the powerful tool for investigating the surface properties of the material and

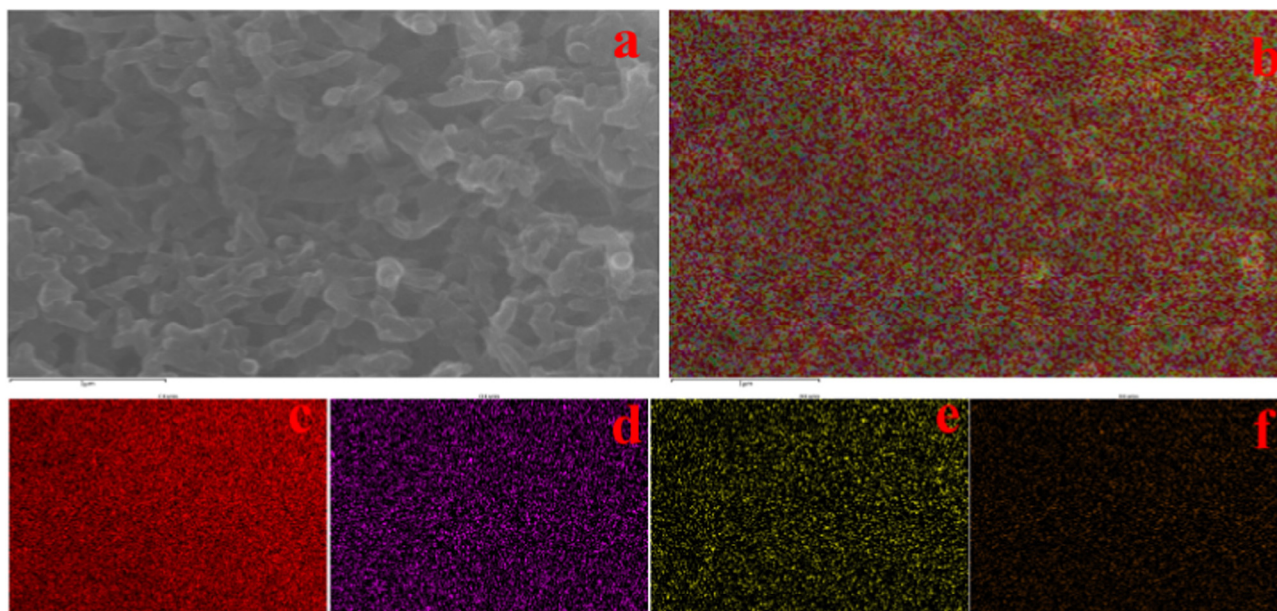


Fig. 4 (a) FESEM image and (b) EDX elemental mapping of P-BN-2 nanocomposite on a Si wafer for the following elements: (c) C, (d) Cl (e) N and (f) Boron.

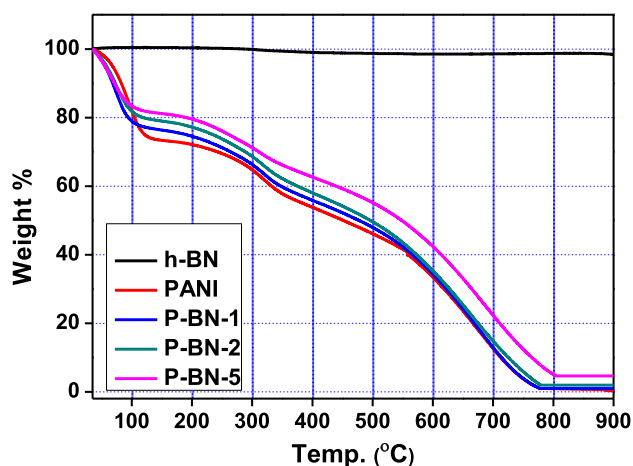


Fig. 5 TGA patterns of h-BN nanosheets, PANI nanotubes and h-BN nanosheets doped nanocomposites.

was used for examining the specific surface area of h-BN nanosheets, PANI nanotubes and h-BN nanosheets doped nanocomposites via computing the nitrogen adsorption–desorption isotherms. Fig. 6 demonstrates the nitrogen adsorption–desorption isotherms of h-BN, PANI nanotubes, P-BN-1, P-BN-2 and P-BN-5. As obvious from Fig. 6, the adsorption–desorption isotherms of the aforementioned materials depicted the distinguishing type-IV isotherms consistent with the International Union of Pure and Applied Chemistry (IUPAC) classification which stipulates their mesoporous nature (Sing, 1985; Yu et al., 2013). The specific surface area for h-BN nanosheets, PANI nanotubes, and the nanocomposites is illustrated in Table 1. As evident from the obtained BET surface area results, the surface area of the nanocomposites was found to be higher than that of bare polymer and h-BN nanosheets. The increment in the surface area may be due to

the changes in the surface morphology of the PANI homopolymer in the presence of h-BN. As discussed in Section 3.1, the surface of the PANI nanotubes has become granular upon doping with h-BN which has increased the porosity of the material and has led to the overall increment in the surface area of the nanocomposites. Additionally, the surface area of the nanocomposites increases with increasing the percentage of h-BN from 1% to 2% and slightly decreases when the doping percentage increase to 5%. This decrease in the surface area upon increasing the concentration of h-BN might be due to the agglomeration of h-BN nanosheets at higher concentration which has decreased the overall surface area of the nanocomposite. Thus, BET investigations revealed the formation of high surface area porous nanocomposites which is a prime requisition for the photocatalyst.

3.4. XRD analysis

The crystal structure and phase of the samples were analysed by X-ray diffraction investigations and are represented in Fig. 7. The XRD pattern of h-BN exhibited very well defined, intense and well separated peaks representing a higher degree of structural ordering. All the obtained peaks at 26.80, 41.70, 42.95, 50.20, 55.28, 71.41, 75.98 and 82.27 can be readily indexed to expected crystallographic planes of pure h-BN (0 0 2), (1 0 0), (1 0 1), (1 0 2), (0 0 4), (1 0 4), (1 1 0), and (1 1 2) respectively in accordance with the JCPDS file number 01-073-2095 (Guo et al., 2013; Yuan et al., 2016). The characteristic diffraction peaks of conductive PANI appeared at $2\theta = 15.76$, 20.35, and 25.25 which indicates polycrystalline structure of PANI (Rahy and Yang, 2008). The intense peaks appearing in the XRD spectrum of PANI at the diffraction angles of $2\theta = 20.35$ and 25.25 may be assigned to the periodic repetition of benzenoid and quinoid rings respectively in PANI chains (Shi et al., 2009). As depicted by the XRD pattern of the h-BN nanosheet doped nanocomposites, the sharp and persis-

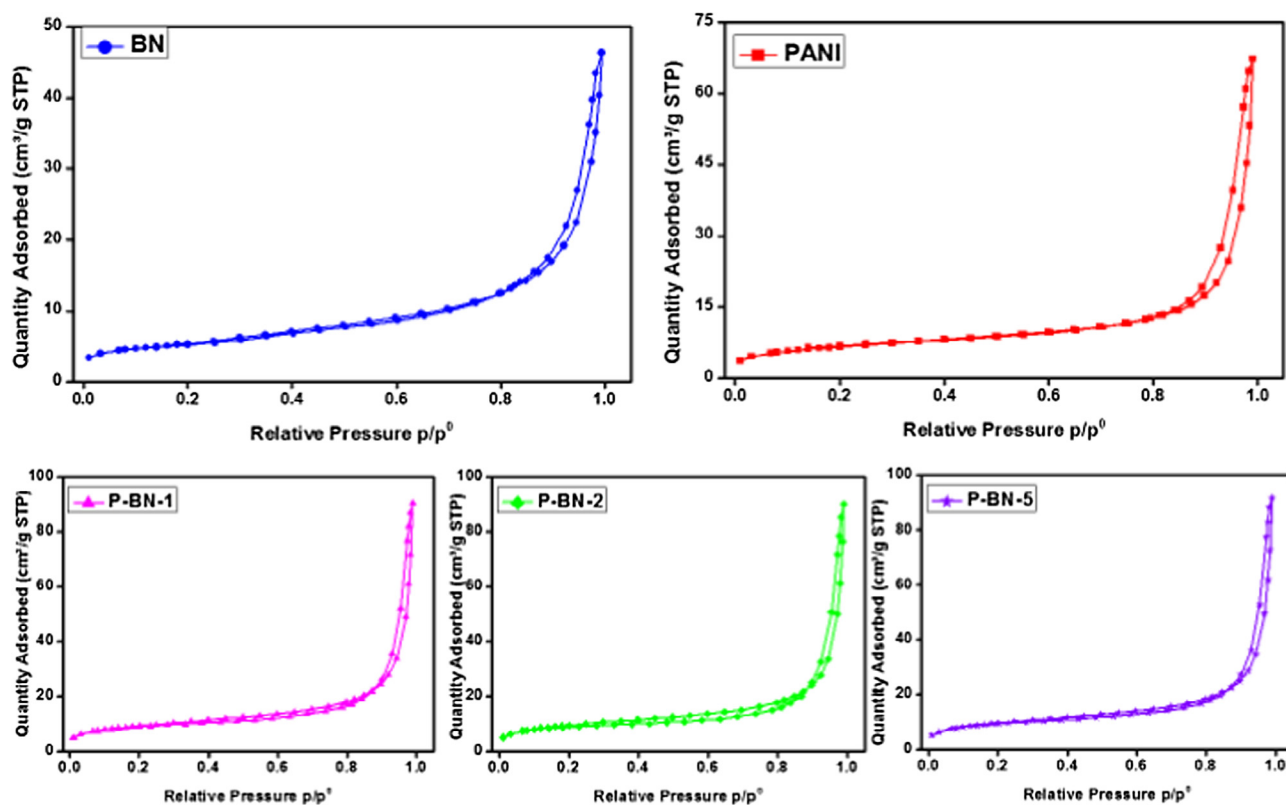


Fig. 6 Nitrogen adsorption–desorption isotherms (BET) of h-BN nanosheets, PANI nanotubes and h-BN nanosheets doped nanocomposites.

Table 1 BET surface area.

BET analysis		
S. no.	Material	BET surface area ($\text{m}^2 \text{g}^{-1}$)
1	h-BN Nanosheets	19.04
2	PANI Nanotubes	24.02
3	P-BN-1	33.67
4	P-BN-2	34.85
5	P-BN-5	34.42

tent peaks of PANI nanotubes were retarded significantly upon the addition of h-BN within the polymer matrix. This decrease in the intensity of peaks of PANI may be ascribed to the fact that h-BN nanosheets acts as an impurity thereby retarding the formation of PANI crystallite. The characteristic peak of h-BN also appeared in the spectra of nanocomposites, slightly shifted and becomes intense with the increase in the amount of h-BN which suggested some interaction within the PANI chains and h-BN nanosheets within the nanocomposites. Hence, XRD investigation indicated the successful synthesis of PANI homopolymer and h-BN nanosheets doped nanocomposites.

3.5. FTIR analysis

Figs. 8 and S2 shows the FT-IR spectra of h-BN nanosheets, PANI nanotubes and the synthesised nanocomposites. As apparent from the FT-IR spectrum of h-BN, the fingerprint

peaks of h-BN appeared at 1352 and 780 cm^{-1} as indicated by the arrows. The peak at 1352 cm^{-1} may be attributed to the in-plane stretching vibrations of B–N bonds whereas the peak appearing at 780 cm^{-1} can be assigned to the out of the plane B–N–B bending vibrations (Salehirad and Nikje, 2017; Gorbachev et al., 2011; Seyhan et al., 2017). The FT-IR data for PANI nanotubes exhibited the characteristic IR peaks at 1562 cm^{-1} and 1481 cm^{-1} which could be allocated to the representative C–C stretching of quinoid and benzenoid rings in PANI homopolymer, respectively (Arasi et al., 2009). The IR peak representative to C–N and C=N stretching in PANI nanotubes appeared at 1290 cm^{-1} whereas peaks at 1120 and 808 cm^{-1} may be ascribed to in-plane C–H bending and out-of-plane C–H bending in PANI chains (Syed, 2016; Shahabuddin et al., 2016c). The FT-IR spectra of h-BN nanosheets doped nanocomposites are depicted in Fig. S4 which shows the characteristic IR peaks of PANI nanotubes with a slight shifting in the band after doping of PANI nanotubes with h-BN. The IR band of 1550 is shifted to around 1532 cm^{-1} whereas the band at 1481 appeared at around 1380 cm^{-1} . This slight shifting of the IR bands toward the red side of the spectrum may be due to the weak interactions such as Van der Waals attraction between the positively charged PANI backbones and the h-BN molecules. Also, the characteristic peaks of h-BN at 1295 cm^{-1} and 791 cm^{-1} start to appear within the spectra of the nanocomposites (marked by arrows) and the intensities of these peaks increases with the increase in the doping percentage of h-BN. Thus, FT-IR results supports the formation of h-BN nanosheets doped nanocomposites successfully.

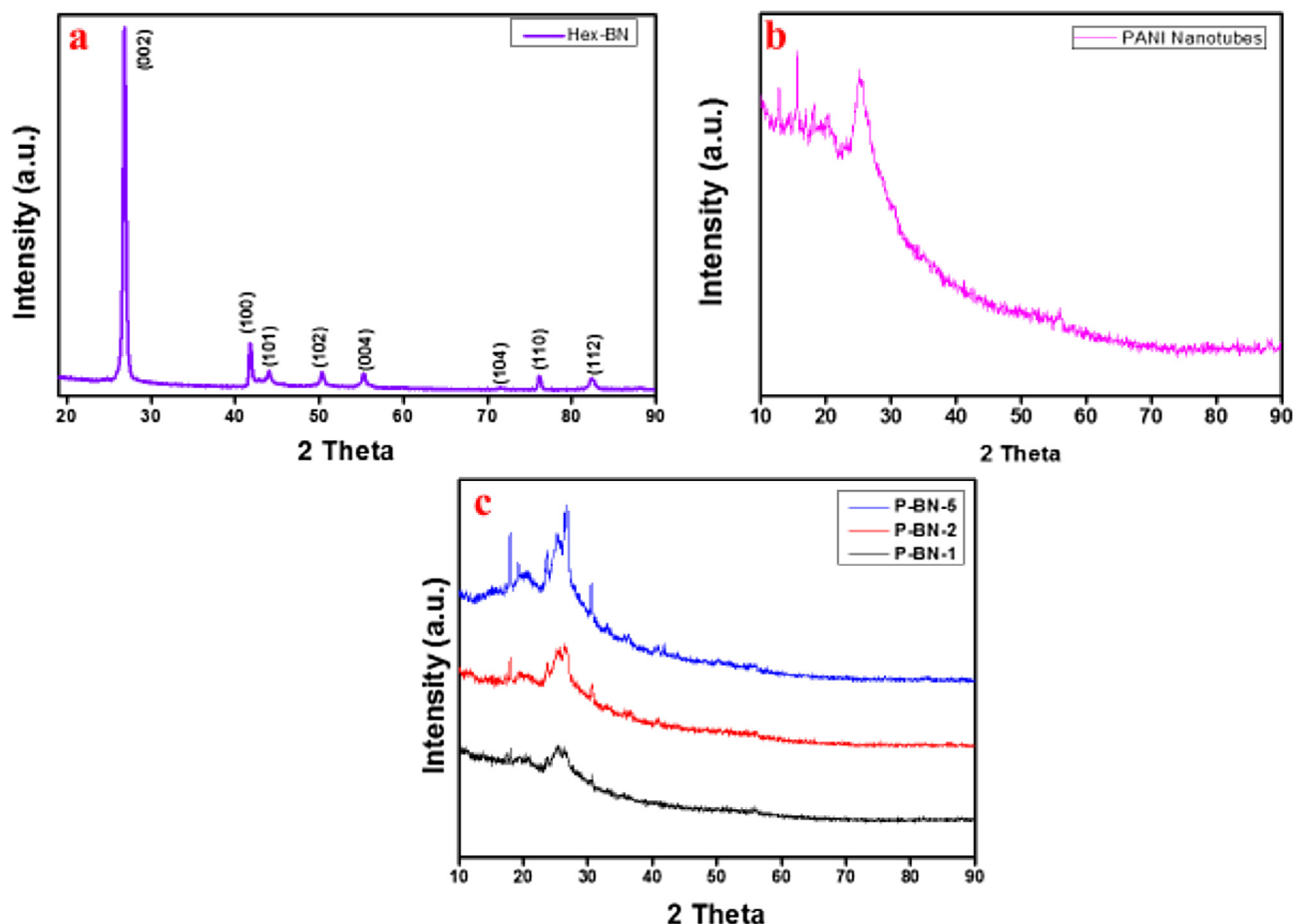


Fig. 7 XRD patterns of (a) h-BN nanosheets, (b) PANI nanotubes and (c) h-BN nanosheets doped nanocomposites.

3.6. Photocatalytic degradation of MB under UV irradiation

The aqueous-phase photocatalytic degradation studies for MB and MO were performed using UV-light illumination at ambient temperature in the presence of h-BN nanosheets, PANI nanotubes and h-BN nanosheets doped nanocomposites namely, P-BN-1, P-BN-2 and P-BN-5. The adsorption-desorption equilibrium under dark conditions for the adsorption of MB and MO on the surface of the catalysts was observed for 75 min using via UV-vis absorption technique as depicted in Fig. 9. As apparent from Fig. 9(a) and (b), with increment in the adsorption time, the amount of MB molecules adsorbed on the surface of catalysts increases and the catalyst surface attained saturation with dye molecules within 45 min of dark adsorption. Same trend was observed in the dark adsorption-desorption equilibrium attainment of MO dye where the catalyst saturation was achieved within 60 min approximately as can be seen from Fig. 9(c) and (d). After dark adsorption-desorption equilibrium attainment approximately 2.3%, 10.8%, 15.75%, 19.90% and 21.80% of MB and 1.9%, 11.1%, 17.8%, 23% and 21.3% of MO was adsorbed on the surface of h-BN nanosheets, PANI nanotubes, P-BN-1, P-BN-2 and P-BN-5 respectively. The dye molecules (MB and MO) are adsorbed on the surface of conductive PANI nanotubes and its nanocomposites due to electrostatic interactions and π - π conjugation among the

aromatic rings of dye molecules and PANI nanotubes polymeric chains which leads to the enhancement in the adsorption capacity. Moreover, the adsorption was found to be higher in nanocomposites as compared to bare PANI nanotubes which may be due to molecular interactions of the h-BN nanosheets with dye molecules.

The rate and percentage of photodegradation of MB and MO in the presence of h-BN nanosheets, PANI nanotubes, P-BN-1, P-BN-2 and P-BN-5 at varying time intervals are depicted in Fig. 10(a)–(d). As can be seen from Fig. 10(a) and (b), h-BN and PANI nanotubes displayed lower photocatalytic activities as compared to their hybrid nanocomposites, P-BN-1, P-BN-2 and P-BN-5 for the degradation of MB. The percentage degradation as illustrated in Fig. 10(b) depicts the following trend: P-BN-2 > P-BN-5 > P-BN-2 > PANI nanotubes > h-BN nanosheets. Similar photocatalytic behaviour has been observed in the degradation of MO with Fig. 10(c) and (d) exhibiting maximum photocatalytic efficiency of P-BN-2 followed by P-BN-5, P-BN-2, PANI nanotubes and h-BN nanosheets. Figs. 11 and 12 shows the real time UV-vis adsorption spectra of h-BN, PANI nanotubes and h-BN doped nanocomposites irradiated under UV illumination for different time intervals for MB and MO respectively. These real time photocatalytic degradation curves indicate the enhanced degradation of MB and MO through photocatalytic phenomenon. The intensity of the MB adsorption band

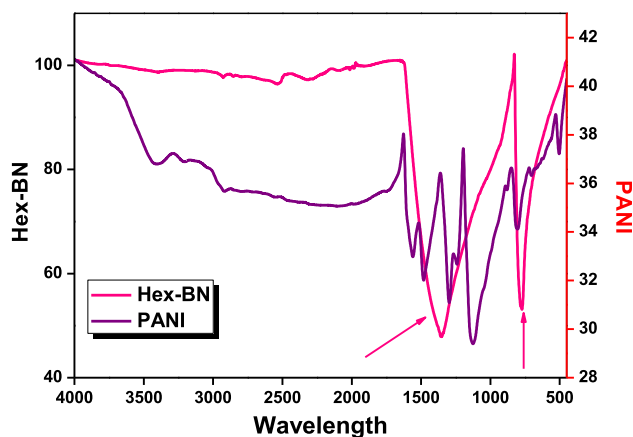


Fig. 8 FTIR spectrum of h-BN nanosheets and PANI nanotubes.

decreases significantly with increasing irradiation time. However, this decrease in the intensity of adsorption band for MB shows different trends with different material. For instance, h-BN nanosheets (Fig. 11(a)) does not show any significant photocatalytic activity with only 4.2% of degrada-

tion within 90 min. On the contrary, PANI nanotubes demonstrates some photocatalytic phenomenon with 32% photodegradation of MB after 90 min as can be seen from Fig. 11(b). Fig. 11(c)–(e), reveals the degradation pattern for P-BN-1, P-BN-2 and P-BN-5 which depicts the significantly enhanced photocatalytic efficiencies as compared to bare PANI homopolymer. The comparison of photocatalytic activities of all the photocatalysts is exhibited in Fig. 11(f) which shows the UV–vis adsorption spectra of the of h-BN, PANI nanotubes and h-BN doped nanocomposites at the 90th minute of irradiation. The data reveals that P-BN-2 degraded 93% of MB whereas P-BN-1 and P-BN-5 degraded 68 and 87 percent of MB after 90 min of irradiation, respectively. The photocatalytic degradation data of MO is represented in Fig. 12(a)–(f). Photocatalytic degradation of MO also shows similar pattern as depicted by MB degradation. Approximately 95% of MO was degraded in 90 min by P-BN-2 followed by 89%, 79%, 38% and 5.1% photodegradation by P-BN-5, P-BN-1, PANI nanotubes and h-BN. The photocatalytic analysis of the MB and MO dye under UV-photoillumination revealed that PANI can degrade certain amount of organic matter due to the presence of conducting polymeric chains undergoing π - π^* transitions upon photoirradiation. However, the photocatalytic degradation efficiency increases significantly upon

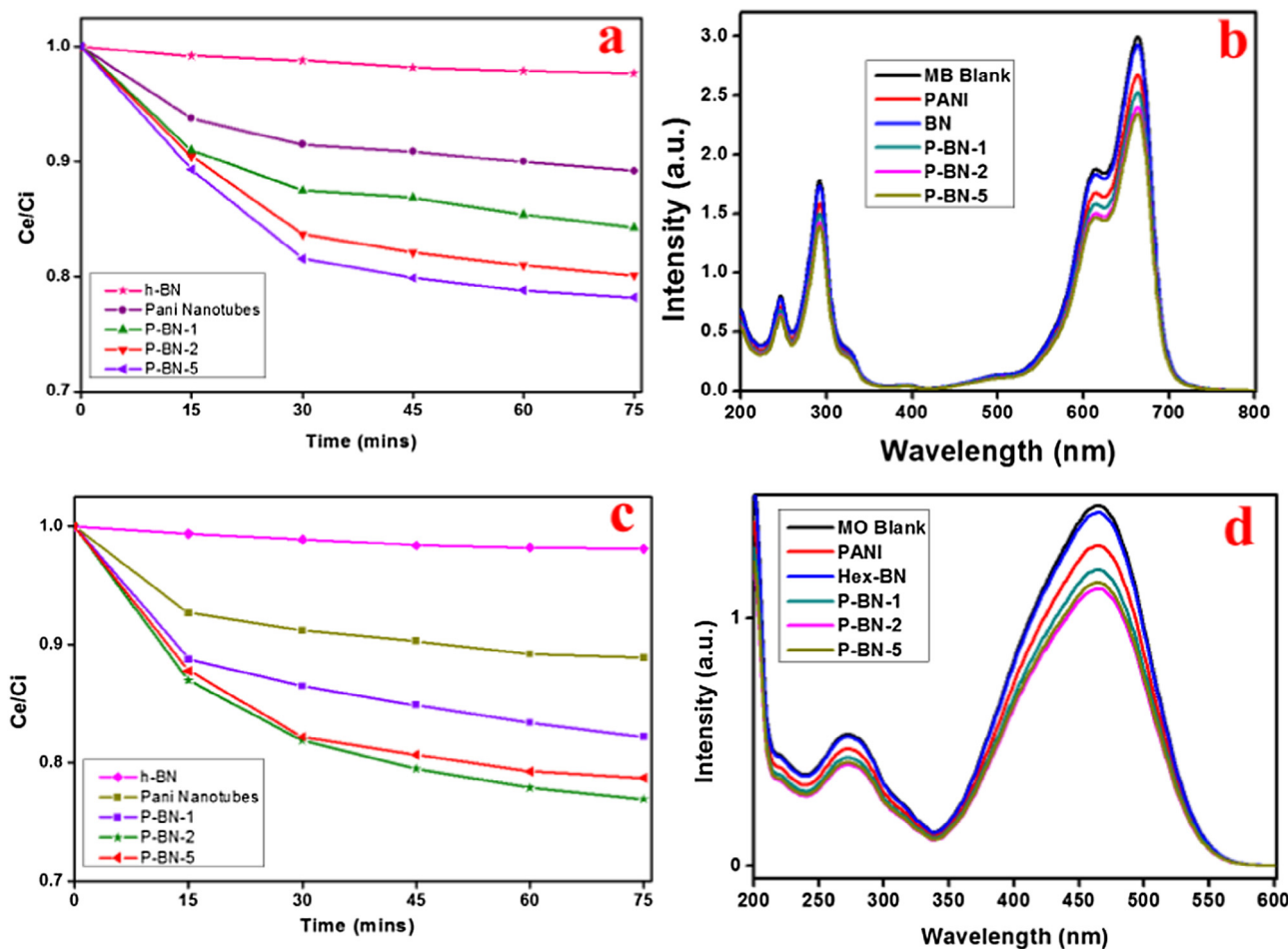


Fig. 9 (a) and (c) Adsorption–desorption equilibrium rate of MB and MO under dark conditions versus time in the presence of various photocatalysts (b) and (d) UV–vis absorption spectra of MB and MO aqueous solution at 75-min dark adsorption–desorption equilibrium.

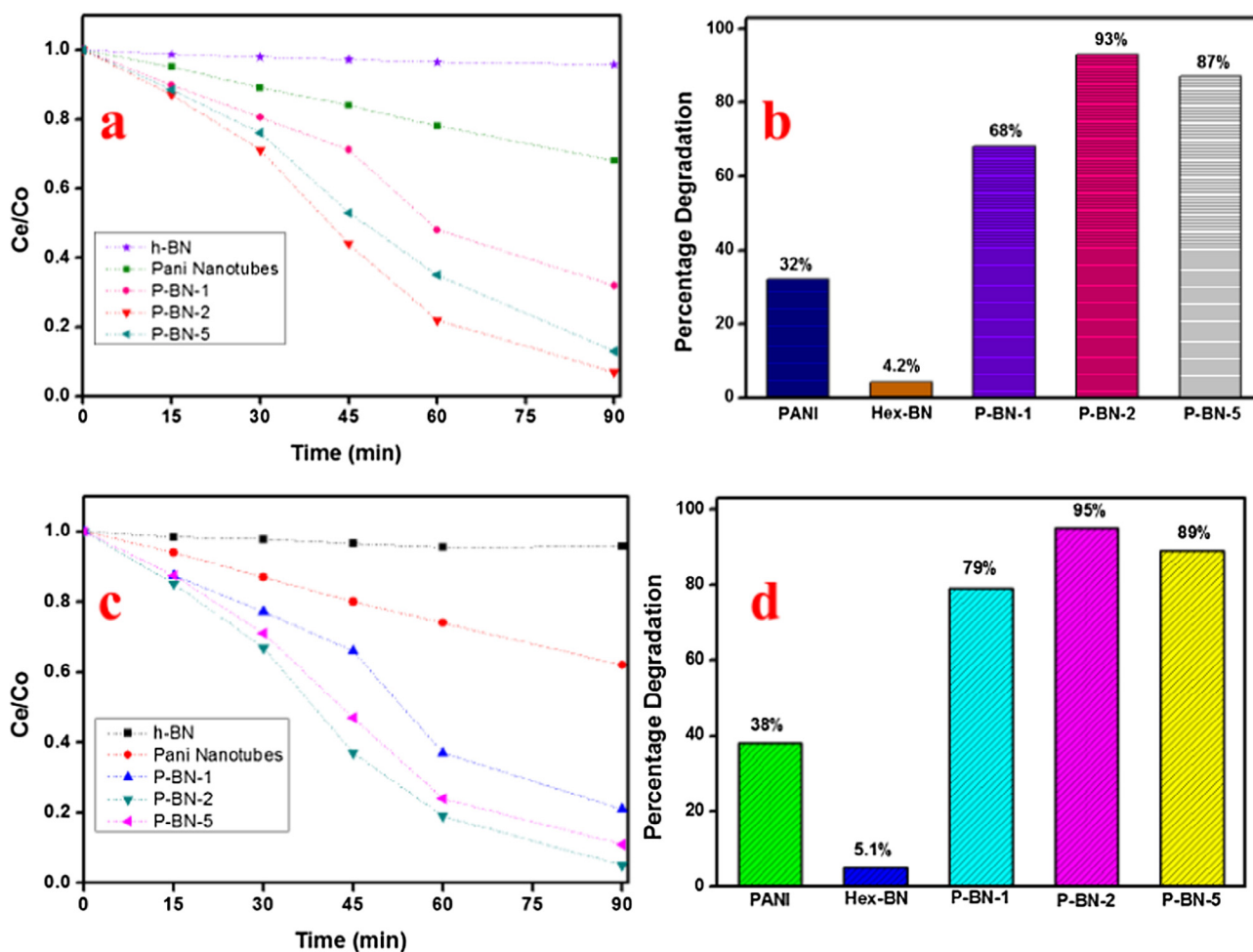


Fig. 10 (a) and (c) Photodegradation rate of MB and MO at different time intervals in the presence of various photocatalysts (b) and (d) Percentage degradation of MB and MO in the presence of various photocatalysts.

doping of PANI with h-BN nanosheets. The photocatalytic efficiency increased noticeably upon increasing the concentration of h-BN from 1% to 2% but shows a slight decrease on further increasing the concentration of h-BN from 25 to 5%. This might be due to the fact that at higher concentration of h-BN nanosheets, agglomeration of nanosheets takes place which decreases the effective surface area of the photocatalyst thereby hampering the overall photocatalytic efficacy. This reduction in surface area is also supported by BET analysis, thereby envisaging P-BN-2 to be an optimal photocatalyst composition.

The organic dyes have the tendency to absorb light upon illumination and undergoes electronic transition accompanied by intersystem crossing which is responsible for generation of singlet and triplet species thereby leading their self-decomposition (Subramanian et al., 2014). The singlets and triplets species formed due to photoexcitation are highly energetic and reactive which upon reaction with oxygen and water molecules forms peroxide, superoxide, and hydroxyl radicals. These radicals are generally known as advanced oxidation species (AOS) which are the real scavengers and degrade any organic moiety such as dye molecules and other pollutants which comes in contact with them. However, this photo-phenomenon by the dyes is insignificant with only a

very little fraction of photodegradation and is usually augmented by using efficient photocatalysts. The AOS can also be generated by conductive PANI and its various hybrid nanocomposites with higher band gap semiconducting materials leading to the efficient and enhanced degradation of organic pollutants. The conductive emeraldine state of PANI homopolymer has demonstrated higher electron mobility where the electrons can be easily excited by photoirradiation. Analogous to various conductors and semiconductors, emeraldine state of PANI have its own valence and conduction bands commonly known as HOMO (Highest Occupied Molecular Orbital) and LUMO (Lowest Unoccupied Molecular Orbital). The valence electrons present in HOMO can be excited by absorbing energy from photons when illuminated by light source thereby jumping to LUMO via $\pi-\pi^*$ transitions, the characteristic transitions of PANI molecules (Shahabuddin et al., 2016a, 2015). Due to these electronics transitions within the matrix of conductive PANI polymeric chains electrons and holes are formed in the HOMO and LUMO of PANI respectively, which further forms AOS by reacting with medium's water and oxygen molecules leading to the degradation of MB and MO molecules. This process however is not very efficient since rapid recombination of holes and electrons takes place which limits the formation of AOS and thus significantly

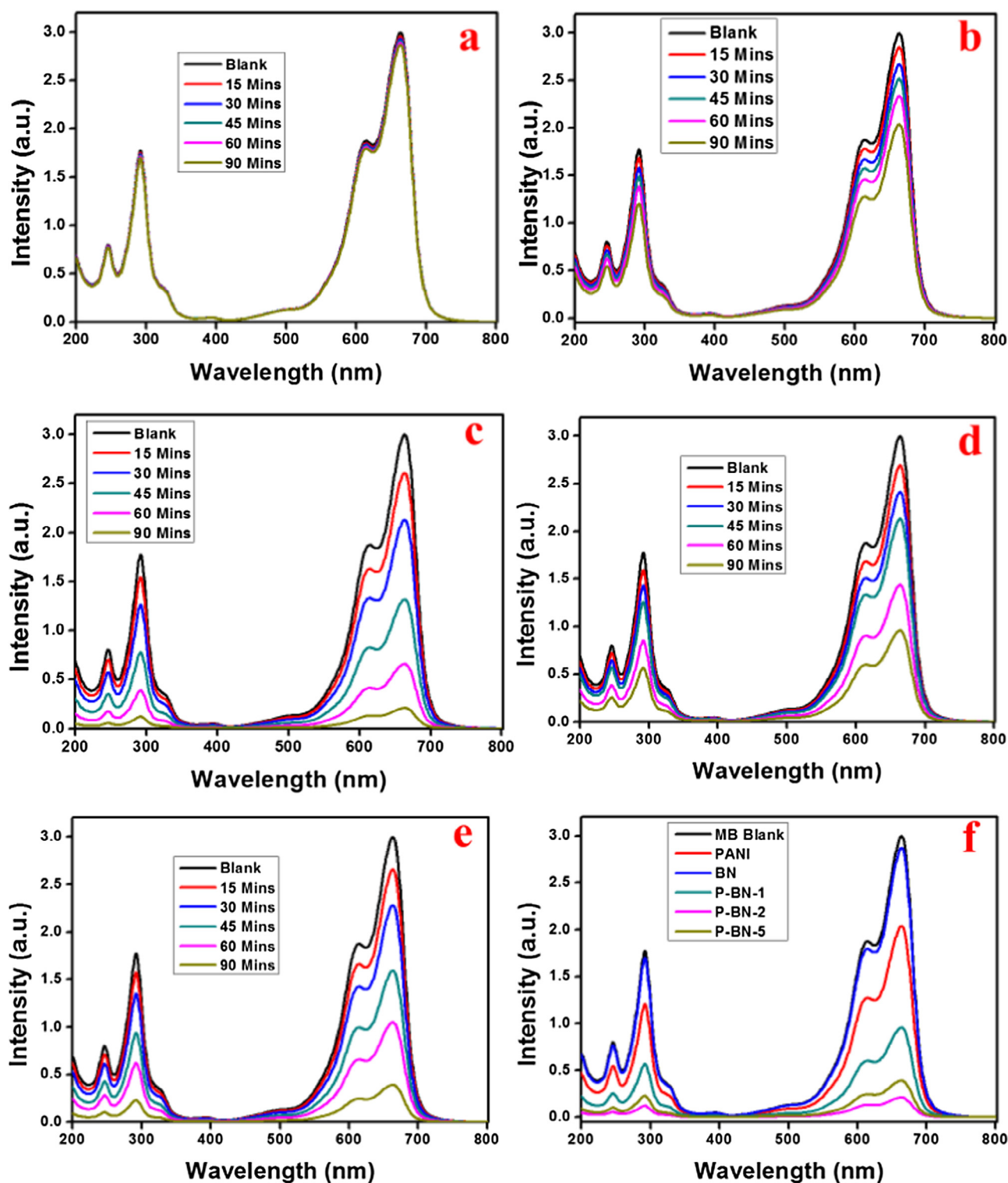


Fig. 11 UV-vis absorption spectra of MB aqueous solution at different times in the presence of (a) h-BN nanosheets (b) PANI Nanotubes (c) P-BN-1 (d) P-BN-2 (e) P-BN-5 and (f) UV-vis absorption spectra of MB photodegradation at 90th minute in presence of different photocatalyst.

decreases the photocatalytic efficiency of PANI homopolymer. In order to improve the photocatalytic efficiency of PANI homopolymer semiconducting h-BN nanosheets were incorporated within the chains of PANI polymer via simple in-situ

polymerization technique. h-BN is a wide band gap semiconducting material ($E_g = 5.9\text{--}6.1\text{ eV}$) whereby its conduction band interacts with the LUMO of PANI when upon photoexcitation (Watanabe et al., 2004). These electronic interactions

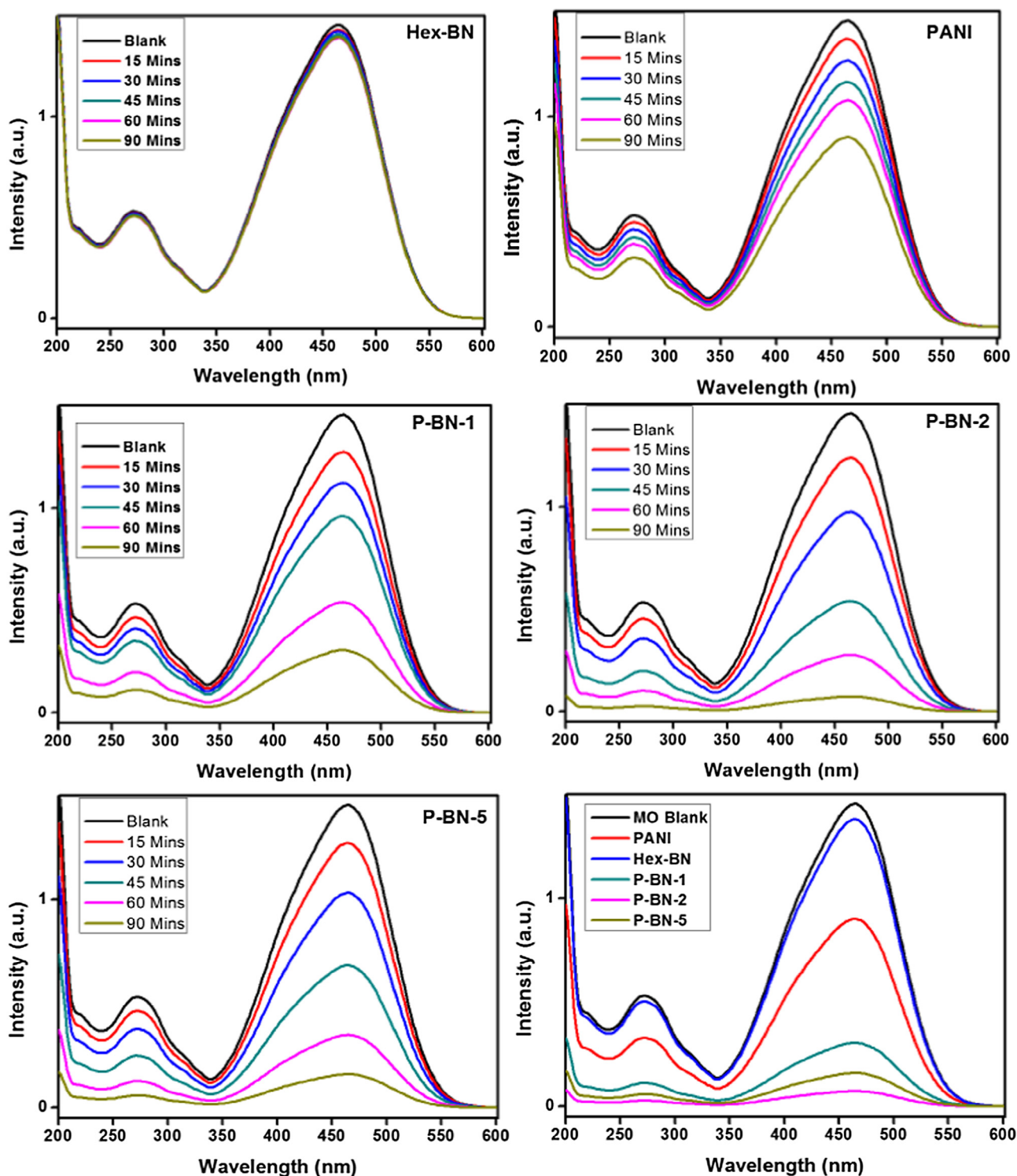


Fig. 12 UV-vis absorption spectra of MO aqueous solution at different times in the presence of (a) h-BN nanosheets (b) PANI Nanotubes (c) P-BN-1 (d) P-BN-2 (e) P-BN-5 and (f) UV-vis absorption spectra of MO photodegradation at 90th minute in presence of different photocatalyst.

among the LUMO and conduction band of h-BN are responsible for bringing LUMO of PANI to closer to the conducting band of h-BN. Thus, when the nanocomposite comprising PANI chains and h-BN is subjected to irradiations, electrons are excited from the HOMO of PANI and jump to LUMO

leading to the formation of positively charged holes in HOMO. When these photoelectrons are returning to the HOMO for recombination, they come across the empty conduction band of h-BN. Thus, instead of returning back to the HOMO of PANI, these photoelectrons are injected to the empty conduc-

tion bands of h-BN. This phenomenon aids in charge separation and significantly decrease the electron-hole recombination and substantially enhances the formation of AOS. Thus, greater charge separation, lower electron-hole recombination and enhanced formation of AOS leads to the incredible degradation of MB and MO. The plausible mechanism for photodegradation is illustrated by Fig. 13. Consequently, h-BN nanosheets and PANI nanotubes works synergistically for the generation of AOS by hampering electron-hole recombination and boosting charge separation which leads to the formation of an effective photocatalyst for enhanced degradation of MB and MO.

3.7. Comparison of photocatalytic efficiencies

The photocatalytic performance of the synthesised h-BN nanosheet doped nanocomposite is compared with other reported nanocomposites and is illustrated in Table 2. In present investigation, 93% and 95% photocatalytic degradation of MB and MO respectively, is reported with 20 mg/100 mL of catalyst loading at an initial dye concentration of 10 ppm. As apparent from the comparative data from Table 2, the synthesised h-BN nanosheet doped nanocomposite offers enhanced photodegradation within a short interval of time and thus can be applicable for efficient treatment of polluted water and can address the challenge of environmental pollution.

3.8. Reusability studies

Reusability of the photocatalyst is an important aspect which indicates the economic viability and practical usability of the material in real time applications. Therefore, reusability

studies were performed for h-BN nanosheet doped nanocomposite, P-BN-2 as depicted in Fig. 14 for MB and MO photodegradation. The photocatalyst after the first photocatalytic cycle was recovered by subjecting to centrifugal separation and repeated washings with DI water to remove the adsorbed dye molecules. The recovered photocatalyst was then dried in a vacuum oven over a period of 2 h at 80° C and later used for subsequent cycles so as to analyse the photocatalytic efficiencies with repeated cycles. The obtained photocatalytic data reveals that the photocatalytic efficiency of P-BN-2 decreases with each cycle for MB and MO degradation. As apparent from Fig. 14, the percentage degradation of MB was found to be 86%, 81.3%, 78.1% and 74.2% while for MO it was calculated to be 90.2%, 87%, 82.5% and 78% for second, third, fourth and fifth cycle respectively. Thus, the reusability investigations indicated that 74.2% of MB and 78% of MO can still be degraded even after 5th cycle showing the enhanced stability and reusability efficacy of P-BN-2 photocatalyst.

4. Conclusion

In summary, the present investigation epitomised a simple method to develop conducting polymer-based nanocomposites for photocatalytic application using in-situ oxidative polymerisation route. The newly developed photocatalysts revealed higher degree of photocatalytic degradation of MB and MO dyes. The surface morphology reveals the nanotubular nanocomposite formation with enhanced surface area and higher thermal stability. The incorporation of h-BN nanosheets within the matrix of PANI nanotubes indicated the synergistic phenomenon leading to enhancement of charge separation thereby increasing the photocatalysis performance of the nanocomposites. The h-BN doped nanocomposites

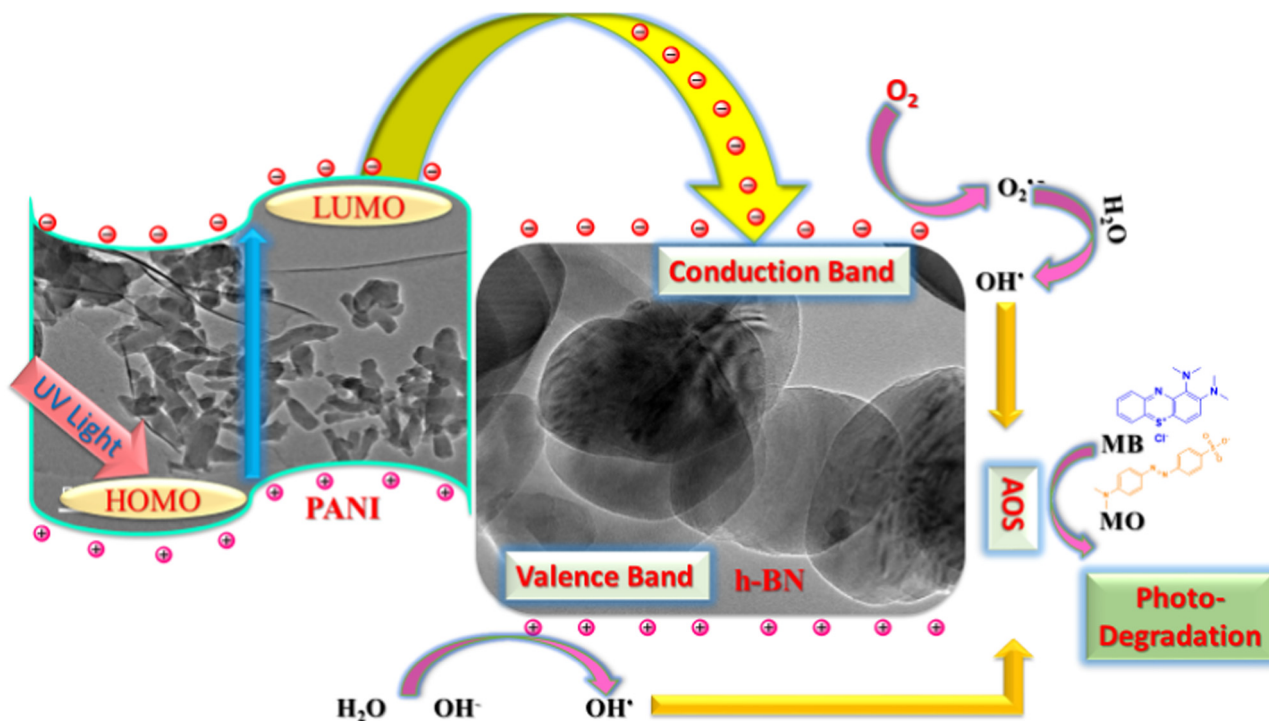


Fig. 13 Schematic illustration for the formation of advanced oxidation species in h-BN nanosheets doped PANI nanocomposite.

Table 2. Comparative study of the photocatalytic efficiencies of the different photocatalysts (Shahabuddin et al., 2016c, 2015; Golsheikh et al., 2015; Liu et al., 2014; Jeghan and Kang, 2017; Sboui et al., 2017; Kim et al., 2016; Eskizeybek et al., 2012; Xia et al., 2015).

Photocatalyst	Model dye	Conc. of dye (mg/L ⁻¹)	Amount of catalyst (mg/ml)	% Degradation	Degradation time (min.)	Source of light	Reference
PANI/TiO ₂ /SiO ₂ membrane	Methyl Orange	1.5	–	87	90	Visible light	Liu et al. (2014)
Graphene/ZnS	Methylene Blue	10	0.2	95	180	UV	Golsheikh et al. (2015)
Urachin like CuCo ₂ O ₄	Methyl Orange	10	0.6	100	240	Sunlight	Jeghan and Kang (2017)
Chitosan/PANI/Co ₃ O ₄	Methylene Blue	10	0.3	88	180	UV	Shahabuddin et al. (2015)
TiO ₂ -PANI/Cork	Methyl Orange	15	1	95	210	Natural sunlight	Sboui et al. (2017)
PANI/SrTiO ₃	Methylene Blue	10	0.3	97	90	Visible light	Shahabuddin et al. (2016c)
Hollow CoFe ₂ O ₄ -PANI nanofibers	Methyl Orange	20	0.2	85	120	LED	Kim et al. (2016)
PANI/ZnO	Methylene Blue	3.2	0.4	99	300	Sunlight	Eskizeybek et al. (2012)
FeOOH-LDO	Methylene Blue	3	35	95	180	Visible light	Xia et al. (2015)
PANI/h-BN	Methylene Blue	10	0.2	93	90	UV	This work
	Methyl Orange	10	0.2	95	90		

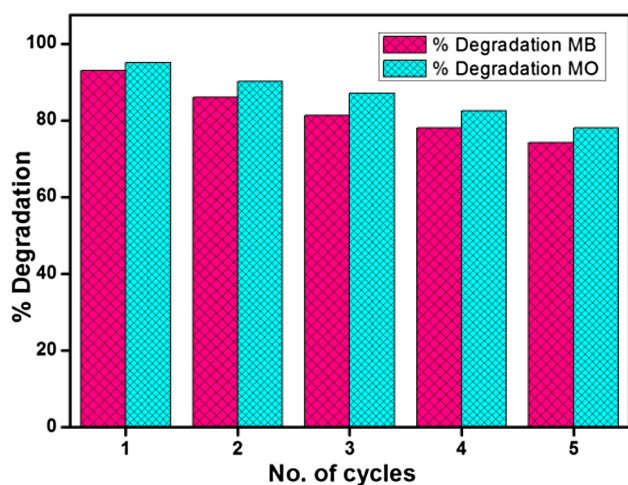


Fig. 14 Reproducibility cycles of P-BN-2 for (a) MB and (b) MO degradation.

demonstrated higher degradation of MB and MO within short interval of time as compared with the pure PANI nanotubes and h-BN. The reusability analysis specified that the synthesised nanocomposite is highly stable even after the 5th cycle and can be effectively reused for longer durations. Additionally, the presented technique is a cost effective and facile methodology which can be exploited for designing several other types of nanocomposites to confront the growing menace of environmental pollution.

Acknowledgements

The authors would like to thank the Sunway University for the research facilities and financial support through internal grant (INT-2018-SST-RCNMET-04).

Appendix A. Supplementary material

Supplementary data associated with this article can be found, in the online version, at <https://doi.org/10.1016/j.arabjc.2018.05.004>.

References

- Adams, V., Marley, J., McCarroll, C., 2007. Prilocaine induced methaemoglobinaemia in a medically compromised patient. Was this an inevitable consequence of the dose administered? *Br. Dent. J.* 203, 585.
- Arasi, A.Y., Jeyakumari, J.J.L., Sundaresan, B., Dhanalakshmi, V., Anbarasan, R., 2009. The structural properties of poly (aniline)—analysis via FTIR spectroscopy. *Spectrochim. Acta Part A: Mol. Biomol. Spectrosc.* 74, 1229–1234.
- Autin, O., Romelot, C., Rust, L., Hart, J., Jarvis, P., MacAdam, J., Parsons, S.A., Jefferson, B., 2013. Evaluation of a UV-light emitting diodes unit for the removal of micropollutants in water for low energy advanced oxidation processes. *Chemosphere* 92, 745–751.
- Baharin, S.N.A., Sarih, N.M., Mohamad, S., Shahabuddin, S., Sulaiman, K., Ma'amor, A., 2016. Removal of endocrine disruptor di-(2-ethylhexyl) phthalate by modified polythiophene-coated magnetic nanoparticles: characterization, adsorption isotherm, kinetic study, thermodynamics. *RSC Adv.* 6, 44655–44667.

- Bhimanapati, G., Glavin, N., Robinson, J., 2016. 2D Boron Nitride: Synthesis and Applications, Semiconductors and Semimetals. Elsevier, pp. 101–147.
- Chan, S.H.S., Yeong Wu, T., Juan, J.C., Teh, C.Y., 2011. Recent developments of metal oxide semiconductors as photocatalysts in advanced oxidation processes (AOPs) for treatment of dye wastewater. *J. Chem. Technol. Biotechnol.* 86, 1130–1158.
- Dai, K., Lv, J., Lu, L., Liu, Q., Zhu, G., Li, D., 2014. Synthesis of micro-nano heterostructure AgBr/ZnO composite for advanced visible light photocatalysis. *Mater. Lett.* 130, 5–8.
- Eskizeybek, V., Sari, F., Gülce, H., Gülce, A., Avcı, A., 2012. Preparation of the new polyaniline/ZnO nanocomposite and its photocatalytic activity for degradation of methylene blue and malachite green dyes under UV and natural sun lights irradiations. *Appl. Catal. B* 119, 197–206.
- Ge, M., Cao, C., Huang, J., Li, S., Chen, Z., Zhang, K.-Q., Al-Deyab, S., Lai, Y., 2016. A review of one-dimensional TiO₂ nanostructured materials for environmental and energy applications. *J. Mater. Chem. A* 4, 6772–6801.
- Golsheikh, A.M., Lim, H., Zakaria, R., Huang, N., 2015. Sonochemical synthesis of reduced graphene oxide uniformly decorated with hierarchical ZnS nanospheres and its enhanced photocatalytic activities. *RSC Adv.* 5, 12726–12735.
- Gorbachev, R.V., Riaz, I., Nair, R.R., Jalil, R., Britnell, L., Belle, B. D., Hill, E.W., Novoselov, K.S., Watanabe, K., Taniguchi, T., 2011. Hunting for monolayer boron nitride: optical and Raman signatures. *Small* 7, 465–468.
- Gouamid, M., Ouahrani, M., Bensaci, M., 2013. Adsorption equilibrium, kinetics and thermodynamics of methylene blue from aqueous solutions using date palm leaves. *Energy Proc.* 36, 898–907.
- Guo, C., Dong, L.M., Gong, S.J., Miao, C.Y., Zhang, X.Y., 2013. Synthesis and characterization of hexagonal boron nitride nanosheets, in: *Applied Mechanics and Materials*, Trans Tech Publ, 2013, pp. 411–414.
- Gupta, V., 2009. Application of low-cost adsorbents for dye removal—a review. *J. Environ. Manage.* 90, 2313–2342.
- Gustafsson, G., Cao, Y., Treacy, G., Klavetter, F., Colaneri, N., Heeger, A., 1992. Flexible light-emitting diodes made from soluble conducting polymers. *Nature* 357, 477.
- Huang, S.-T., Lee, W.W., Chang, J.-L., Huang, W.-S., Chou, S.-Y., Chen, C.-C., 2014. Hydrothermal synthesis of SrTiO₃ nanocubes: characterization, photocatalytic activities, and degradation pathway. *J. Taiwan Inst. Chem. Eng.* 45, 1927–1936.
- Jamal, R., Zhang, L., Wang, M., Zhao, Q., Abdiryim, T., 2016. Synthesis of poly (3,4-propylenedioxythiophene)/MnO₂ composites and their applications in the adsorptive removal of methylene blue. *Progr. Nat. Sci.: Mater. Int.* 26, 32–40.
- Jang, S., Han, M., Im, S., 2000. Preparation and characterization of conductive polyaniline/silica hybrid composites prepared by sol–gel process. *Synth. Met.* 110, 17–23.
- Jang, S.K., Youn, J., Song, Y.J., Lee, S., 2016. Synthesis and characterization of hexagonal boron nitride as a gate dielectric. *Sci. Rep.* 6, 30449.
- Jeghan, S.M.N., Kang, M., 2017. Facile synthesis and photocatalytic activity of cubic spinel urchin-like copper cobaltite architecture. *Mater. Res. Bull.* 91, 108–113.
- Kim, K.K., Hsu, A., Jia, X., Kim, S.M., Shi, Y., Hofmann, M., Nezhich, D., Rodriguez-Nieva, J.F., Dresselhaus, M., Palacios, T., 2011. Synthesis of monolayer hexagonal boron nitride on Cu foil using chemical vapor deposition. *Nano Lett.* 12, 161–166.
- Kim, K.K., Hsu, A., Jia, X., Kim, S.M., Shi, Y., Dresselhaus, M., Palacios, T., Kong, J., 2012. Synthesis and characterization of hexagonal boron nitride film as a dielectric layer for graphene devices. *ACS Nano* 6, 8583–8590.
- Kim, K.N., Jung, H.-R., Lee, W.-J., 2016. Hollow cobalt ferrite–polyaniline nanofibers as magnetically separable visible-light photocatalyst for photodegradation of methyl orange. *J. Photochem. Photobiol., A* 321, 257–265.
- Kobayashi, Y., Akasaka, T., 2008. Hexagonal BN epitaxial growth on (0 0 0 1) sapphire substrate by MOVPE. *J. Cryst. Growth* 310, 5044–5047.
- Liu, Z., Miao, Y.-E., Liu, M., Ding, Q., Tjiu, W.W., Cui, X., Liu, T., 2014. Flexible polyaniline-coated TiO₂/SiO₂ nanofiber membranes with enhanced visible-light photocatalytic degradation performance. *J. Colloid Interf. Sci.* 424, 49–55.
- McCann, J., Ames, B.N., 1976. Detection of carcinogens as mutagens in the Salmonella/microsome test: assay of 300 chemicals: discussion. *Proc. Natl. Acad. Sci.* 73, 950–954.
- Mostafaei, A., Zolriasatein, A., 2012. Synthesis and characterization of conducting polyaniline nanocomposites containing ZnO nanorods. *Progr. Nat. Sci.: Mater. Int.* 22, 273–280.
- Nag, A., Raidongia, K., Hembram, K.P., Datta, R., Waghmare, U.V., Rao, C., 2010. Graphene analogues of BN: novel synthesis and properties. *ACS Nano* 4, 1539–1544.
- Nodeh, M.K.M., Soltani, S., Shahabuddin, S., Nodeh, H.R., Sereshti, H., 2018. Equilibrium, kinetic and thermodynamic study of magnetic polyaniline/graphene oxide based nanocomposites for ciprofloxacin removal from water. *J. Inorg. Organomet. Polym Mater.*, 1–9.
- Parida, K., Sahu, S., Reddy, K., Sahoo, P., 2010. A kinetic, thermodynamic, and mechanistic approach toward adsorption of methylene blue over water-washed manganese nodule leached residues. *Ind. Eng. Chem. Res.* 50, 843–848.
- Raffainer, I.L., Rudolf von Rohr, P., 2001. Promoted wet oxidation of the azo dye orange II under mild conditions. *Ind. Eng. Chem. Res.* 40, 1083–1089.
- Rahy, A., Yang, D.J., 2008. Synthesis of highly conductive polyaniline nanofibers. *Mater. Lett.* 62, 4311–4314.
- Ray, S.S., Biswas, M., 2000. Water-dispersible conducting nanocomposites of polyaniline and poly (N-vinylcarbazole) with nanodimensional zirconium dioxide. *Synth. Met.* 108, 231–236.
- Salehirad, M., Nikje, M.M.A., 2017. Synthesis and characterization of exfoliated polystyrene grafted hexagonal boron nitride nanosheets and their potential application in heat transfer nanofluids. *Iran. Polym. J.* 26, 467–480.
- Sboui, M., Nsib, M.F., Rayes, A., Swaminathan, M., Houas, A., 2017. TiO₂–PANI/Cork composite: a new floating photocatalyst for the treatment of organic pollutants under sunlight irradiation. *J. Environ. Sci.* 60, 3–13.
- Seyhan, A.T., Göncü, Y., Durukan, O., Akay, A., Ay, N., 2017. Silanization of boron nitride nanosheets (BNNs) through microfluidization and their use for producing thermally conductive and electrically insulating polymer nanocomposites. *J. Solid State Chem.* 249, 98–107.
- Shahabuddin, S., Sari, N.M., Ismail, F.H., Shahid, M.M., Huang, N. M., 2015. Synthesis of chitosan grafted-polyaniline/Co₃O₄ nanocube nanocomposites and their photocatalytic activity toward methylene blue dye degradation. *RSC Adv.* 5, 83857–83867.
- Shahabuddin, S., Sari, N.M., Mohamad, S., Baharin, S.N.A., 2016a. Synthesis and characterization of Co₃O₄ nanocube-doped polyaniline nanocomposites with enhanced methyl orange adsorption from aqueous solution. *RSC Adv.* 6, 43388–43400.
- Shahabuddin, S., Muhamad Sari, N., Mohamad, S., Joon Ching, J., 2016b. SrTiO₃ nanocube-doped polyaniline nanocomposites with enhanced photocatalytic degradation of methylene blue under visible light. *Polymers* 8, 27.
- Shahabuddin, S., Sari, N.M., Afzal Kamboh, M., Rashidi Nodeh, H., Mohamad, S., 2016c. Synthesis of polyaniline-Coated graphene oxide@ SrTiO₃ nanocube nanocomposites for enhanced removal of carcinogenic dyes from aqueous solution. *Polymers* 8, 305.
- Shi, L., Wang, X., Lu, L., Yang, X., Wu, X., 2009. Preparation of TiO₂/polyaniline nanocomposite from a lyotropic liquid crystalline solution. *Synth. Met.* 159, 2525–2529.

- Sing, K.S., 1985. Reporting physisorption data for gas/solid systems with special reference to the determination of surface area and porosity (Recommendations 1984). *Pure Appl. Chem.* 57, 603–619.
- Singh, D.P., 2010. Synthesis and growth of ZnO nanowires. *Sci. Adv. Mater.* 2, 245–272.
- Snyder, E.G., Watkins, T.H., Solomon, P.A., Thoma, E.D., Williams, R.W., Hagler, G.S., Shelow, D., Hindin, D.A., Kilaru, V.J., Preuss, P.W., 2013. *The Changing Paradigm of Air Pollution Monitoring*. ACS Publications.
- Song, L., Liu, Z., Reddy, A.L.M., Narayanan, N.T., Taha-Tijerina, J., Peng, J., Gao, G., Lou, J., Vajtai, R., Ajayan, P.M., 2012. Binary and ternary atomic layers built from carbon, boron, and nitrogen. *Adv. Mater.* 24, 4878–4895.
- Srivastava, V., Maydannik, P., Sharma, Y., Sillanpää, M., 2015. Synthesis and application of polypyrrole coated tenorite nanoparticles (PPy@ TN) for the removal of the anionic food dye 'tartrazine' and divalent metallic ions viz. Pb (II), Cd (II), Zn (II), Co (II), Mn (II) from synthetic wastewater. *RSC Adv.* 5, 80829–80843.
- Subramanian, E., Subbulakshmi, S., Murugan, C., 2014. Inter-relationship between nanostructures of conducting polyaniline and the photocatalytic methylene blue dye degradation efficiencies of its hybrid composites with anatase TiO₂. *Mater. Res. Bull.* 51, 128–135.
- Syed, S., 2016. *Polyaniline based Nanocomposites as Adsorbents and Photocatalysts in the Removal of Organic Dyes*/Syed Shahabuddin. University of Malaya.
- Vinothkannan, M., Karthikeyan, C., Kim, A.R., Yoo, D.J., 2015. One-pot green synthesis of reduced graphene oxide (RGO)/Fe₃O₄ nanocomposites and its catalytic activity toward methylene blue dye degradation. *Spectrochim. Acta Part A: Mol. Biomol. Spectrosc.* 136, 256–264.
- Wang, F., Min, S., Han, Y., Feng, L., 2010. Visible-light-induced photocatalytic degradation of methylene blue with polyaniline-sensitized TiO₂ composite photocatalysts. *Superlattices Microstruct.* 48, 170–180.
- Watanabe, K., Taniguchi, T., Kanda, H., 2004. Direct-bandgap properties and evidence for ultraviolet lasing of hexagonal boron nitride single crystal. *Nat. Mater.* 3, 404.
- Xia, S., Zhang, L., Pan, G., Qian, P., Ni, Z., 2015. Photocatalytic degradation of methylene blue with a nanocomposite system: synthesis, photocatalysis and degradation pathways. *PCCP* 17, 5345–5351.
- Xing, Z., Zhang, J., Cui, J., Yin, J., Zhao, T., Kuang, J., Xiu, Z., Wan, N., Zhou, W., 2017. Recent advances in floating TiO₂-based photocatalysts for environmental application. *Environ. Appl. Catal. B*.
- Yu, L., Ruan, H., Zheng, Y., Li, D., 2013. A facile solvothermal method to produce ZnS quantum dots-decorated graphene nanosheets with superior photoactivity. *Nanotechnology* 24, 375601.
- Yuan, S., Linas, S., Journet, C., Steyer, P., Garnier, V., Bonnefont, G., Brioude, A., Toury, B., 2016. Pure & crystallized 2D Boron Nitride sheets synthesized via a novel process coupling both PDCs and SPS methods. *Sci. Rep.* 6, 20388.
- Zare, E.N., Motahari, A., Sillanpää, M., 2018. Nanoadsorbents based on conducting polymer nanocomposites with main focus on polyaniline and its derivatives for removal of heavy metal ions/dyes: a review. *Environ. Res.* 162, 173–195.
- Zhang, L., Liu, P., Su, Z., 2006. Preparation of PANI–TiO₂ nanocomposites and their solid-phase photocatalytic degradation. *Polym. Degrad. Stab.* 91, 2213–2219.